

PCCP

Accepted Manuscript



This is an *Accepted Manuscript*, which has been through the Royal Society of Chemistry peer review process and has been accepted for publication.

Accepted Manuscripts are published online shortly after acceptance, before technical editing, formatting and proof reading. Using this free service, authors can make their results available to the community, in citable form, before we publish the edited article. We will replace this *Accepted Manuscript* with the edited and formatted *Advance Article* as soon as it is available.

You can find more information about *Accepted Manuscripts* in the [Information for Authors](#).

Please note that technical editing may introduce minor changes to the text and/or graphics, which may alter content. The journal's standard [Terms & Conditions](#) and the [Ethical guidelines](#) still apply. In no event shall the Royal Society of Chemistry be held responsible for any errors or omissions in this *Accepted Manuscript* or any consequences arising from the use of any information it contains.



PCCP

ARTICLE

Ground State Structures of Tantalum Tetraboride and Triboride: an ab initio Study

Shuli Wei,^a Da Li,^a Yunzhou Lv,^a Zhao Liu,^a Chunhong Xu,^a Fubo Tian,^a Defang Duan,^a Bingbing Liu,^a and Tian Cui^a

Received 00th January 20xx,
Accepted 00th January 20xx

DOI: 10.1039/x0xx00000x

www.rsc.org/

Tantalum-boron compounds, which are potential candidates for superhard multifunctional materials, may possess multiple stoichiometries and structures under pressure. Using the first-principle methods, ground-state TaB₃ with monoclinic *C2/m* space group and high-pressure TaB₄ with orthorhombic *Amm2* space group had been found. They are more stable than previously proposed structures. High-pressure boron-rich *Amm2*-TaB₄ can be quenched to ambient pressure. The ground-state *C2/m*-TaB₃ and high-pressure *Amm2*-TaB₄ are two potential ultra-incompressible and hard materials with calculated hardness of 17.02 GPa and 30.02 GPa at ambient pressure, respectively. Detailed electronic structure and chemical bonding analysis proved that the high hardness of *Amm2*-TaB₄ mainly stems from the strong covalent Boron-Boron bonds in graphene-like B layers as well as B-B bonds between layers.

1 Introduction

Recently, many transition metal borides (e.g., PtN₂,^{1,2} IrN₂,^{2,3} FeB₄,⁴ ReB₂,⁵ OsB₂,⁶ WB₄,⁷ and CrB₄,⁸) were successfully synthesized under ambient or high pressure. They show outstanding properties, such as high melting points, extreme hardness, superior electrical and magnetic properties, strong oxidation and acids resistance. And they are expected to be alternative materials of traditional superhard materials (e.g. diamond and cubic boron nitride). Traditional superhard materials have many faults in actually application. For example, diamond can chemically react with ferrous metals at high temperature, creating iron carbides in the process of machining. For c-BN, its hardness is second only to that of diamond. However, it can only be synthesized under the extreme high pressure and high temperature.⁹ These increase synthesizing costs and limit industrial application of c-BN. Novel transition-metal light-element (B, C, N, and O) compounds have good mechanical and chemical properties to overcome the faults of traditional superhard materials. The search of novel transition-metal light-element (B, C, N, and O) compounds has received noticeable attention in condensed matter physics and materials science. The experimentally synthesized ReB₂ has been proven to be superhard materials with hardness of 36.4-48 GPa, which is close to that of c-BN (45 to 50 GPa).⁵ The boron-rich tetraborides ZrB₄¹⁰ has the high hardness of 42.8 GPa for *Cmcm* phase and 42.6 GPa for *Amm2* phase, respectively. Boron-rich WB₄ (*P6₃/mmc*)⁷ and ReB₄¹¹ with simulated hardness of 43 GPa and 37.1-41.6 GPa were reported. These materials have been proposed to be ideal multifunctional materials with possible superhardness. In addition, boron-rich superhard FeB₄ synthesized under high pressure

is a phonon-mediated superconductor with superconducting temperature T_c of 15–20 K.^{4,12} Ta, W, and Re are neighboring 5d transition metals elements in the same period of the table. So tantalum borides can be expected to be potential superhard and multifunctional materials. In the Ta-B system, Ta-rich tantalum boride Ta₂B with tetragonal Al₂Cu-type structure (*I4/mcm*) was reported in experiment.¹³ Subsequently, the crystal structures of *oS8*-TaB (*Cmcm*), *hP12*-TaB₂ (*P6₃/mmc*), *hP3*-TaB₂ (*P6/mmm*), *oS22*-Ta₅B₆ (*Cmmm*), *tP10*-Ta₃B₂ (*P4/mbm*) and *oI14*-Ta₃B₄ (*Immm*) were confirmed theoretically and experimentally.¹⁴⁻²⁰ The TaB₂ with high Young's modulus (500 GPa) was reported in previous study.¹⁵ Yao *et al.* did a systematic study of transition metal borides (V, Nb, and Ta).¹⁸ Geest *et al.* also studied the phase diagram of Ta-B compounds by doing convex hull calculations.¹⁴ Recently, a monoclinic boron-rich TaB₄ (high hardness of 29 GPa) and a high-pressure orthorhombic *Imma*-TaB₃ were predicted.^{21, 22} Although tantalum borides with relatively high melting temperature, hardness, and brittleness can be regarded as a potential superhard material.¹³⁻²⁰ There are limited studies of boron-rich tantalum tetraboride and triboride in theoretical and experimental works. Many fundamental aspects of boron-rich tantalum borides are still not well understood because of their complex chemical behaviors. The crystal structures of tetraboride and triboride are the subject of continuing debate. The detailed knowledge about the crystal structure of tantalum borides is very important for the study of superhard materials.

In this study, the ground-state crystal structures of TaB₃ and TaB₄ are predicted by using the first principles calculations. And we update the global zero-temperature Ta-B phase diagram at pressures up to 100 GPa. Two monoclinic *C2/m*-TaB₃ structures and a high pressure-phase *Amm2*-TaB₄ are found to be more stable than previously proposed structures. The structural stability and mechanical properties of our proposed *C2/m*-TaB₃ and *Amm2*-TaB₄ have been extensively explored. The ground-state *C2/m*-TaB₃ is mechanically and dynamically stable at ambient pressure. And the

^a State Key Laboratory of Superhard Materials, College of Physics, Jilin University, Changchun, 130012, People's Republic of China. Electronic address: cuiitian@jlu.edu.cn

high-pressure stable *Amm2*-TaB₄ can be quenched to ambient pressure. The *Amm2*-TaB₄ is a hard material with low compressibility compared to some previously proposed transition borides. The six-membered boron rings and boron-boron bonds between different layers are very important for the high hardness of *Amm2*-TaB₄.

2 Computation details

The possible candidate structures of Ta-B compounds were searched by the *ab initio* evolutionary algorithm using the variable-composition mode²³ of the USPEX code.²⁴⁻²⁶ The individual structure searching for TaB₃ and TaB₄ within 1-4 formula units (f.u.) in the simulation cell are implemented at 0, 20, 50, 100, and 150 GPa, respectively. During the structure searching, the first generation is produced randomly. The succeeding generations are obtained through heredity (60%), lattice mutation operations (30%), and atom transmutation (20%). The structural optimizations and enthalpy calculations under different pressures were performed by density functional theory (DFT) with the Vienna *ab initio* simulation program (VASP) code.²⁷ The Perdew-Burke-Ernzerhof (PBE) functional with exchange and correlation treated within the generalized gradient approximation (GGA) was adopted.²⁸ The energy cutoff at 650 eV and a k-mesh at $0.03 \times 2\pi \text{ \AA}^{-1}$ zone were chosen by performing accurate convergence tests in Monkhorst-Pack sampling scheme in the electronic Brillouin zone (BZ) integrations to guarantee that enthalpy calculations are well converged with energy differences better within 1 meV/f.u. The convergence tests have been described elsewhere.²⁹⁻³¹ The elastic constants were calculated from evaluation of stress tensor generated small strains, and the bulk modulus (*B*), shear modulus (*G*), Young's modulus (*E*), and Poisson's ratio (ν) were calculated by using Voigt-Reuss-Hill approximation.³² Phonon calculations were performed by the direct supercell approach using the forces obtained by the Hellmann-Feynman theorem.³³ The phonon frequencies for all structures were calculated using the supercell method with the PHONOPY code.³⁴ The theoretical Vickers hardness was estimated by Chen's model,³⁵ $H_v = 2(k^2G)^{0.585} - 3$ where, $k = G/B$ is Pugh's modulus ratio. Formation enthalpy of Ta_xB_y (ΔH) was calculated by the equation of $\Delta H = H(\text{Ta}_x\text{B}_y) - xH(\text{Ta}) - yH(\text{B})$. The *H* means the enthalpy of solid phase, and the *bcc* structure of tantalum and α -B₁₂, γ -B₂₈ and α -Ga phase of boron³⁶ at different pressures were used.

3. Results and discussions

3.1 Phase diagram and stability

Using USPEX code based on *ab initio* evolutionary algorithm, we obtained several competitive candidates of TaB₃ and TaB₄. Two monoclinic TaB₃ phases had been found. The ambient ground-state structure of I-TaB₃ (space group *C2/m*) transforms to high-pressure

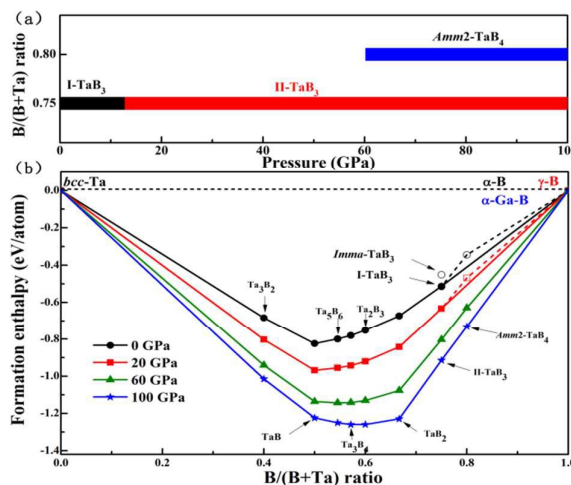


Fig. 1 (a) Pressure versus composition phase diagrams of the TaB₃ and TaB₄ at pressures of 0-100 GPa. (b) Convex hull diagram of Ta-B system at pressures of 0 GPa, 20 GPa, 60 GPa and 100 GPa. Solid symbols denote stable phases while the open represent metastable phases. The α -B (0-19 GPa), γ -B (19-89 GPa), and α -Ga phase (89-100 GPa) were used in the convex calculations.

II-TaB₃ (space group *C2/m*) at 12.5 GPa. And a high-pressure orthorhombic *Amm2*-TaB₄ was predicted. The formation enthalpy of all different phases relative to (Ta + B) was shown in Fig. S1. Thermodynamic stabilities of Ta-B compounds can be described by the knowledge of ground-state enthalpy and formation enthalpy vs composition curve (convex hull).³⁷ It is well known that any structure whose formation enthalpy lies on the convex hull is considered as stable and synthesizable in principle.^{38, 39} The calculated convex hull is depicted in Fig. 1. The pressure versus composition phase diagrams of the TaB₃ and TaB₄ at pressures of 0-100 GPa is inserted in Fig. 1. From the calculated convex hull of Ta-B system, it can be clearly seen that the calculated formation enthalpies of (Ta₃B₂, TaB, Ta₃B₆, Ta₃B₄, Ta₂B₃, and TaB₂) sit nearly right on the curves of convex hull (Fig. 1), in excellent agreement

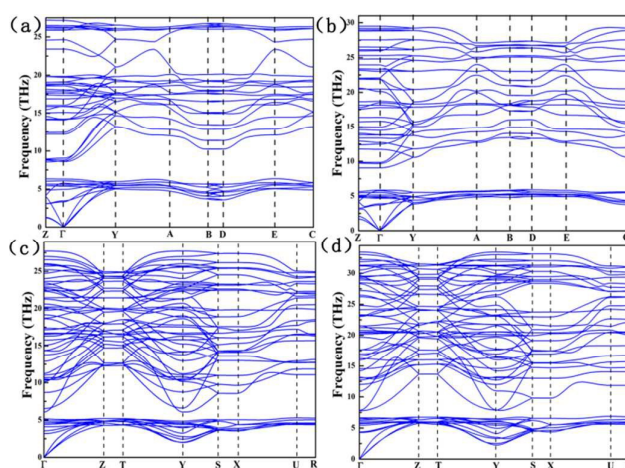


Fig. 2 Phonon dispersion curves of (a) I-TaB₃ at 0 GPa (b) II-TaB₃ at 20 GPa (c) *Amm2*-TaB₄ at 0 GPa and (d) *Amm2*-TaB₄ at 60 GPa.

with the actual experimental syntheses. So our prediction and calculation are reliable. For Boron-rich tantalum borides, trisboride TaB₃ is stable at whole considered pressures, and I-TaB₃ phase is thermodynamically more favorable than other phases up to 12.5 GPa, above which the high-pressure phase II-TaB₃ is energetically more stable, as shown in Fig. S1. The enthalpy curves of all considered structures for TaB₃ in the pressure range of 0–100 GPa were shown in Fig. S1. With further increasing the B:Ta ratio to 4:1, a novel stable structure *Amm2*-TaB₄ is remarkable, and it can be synthesized above 60 GPa, as shown in Fig. 1.

Mechanical and dynamical stabilities are another two indicators to judge existence of structures. The I-TaB₃, II-TaB₃ and *Amm2*-TaB₄ are mechanically stable according to the Born-Huang criterion,⁴⁰ studied hereafter. The phonon calculations provide strict measure for structural dynamic stability. We thus have carefully performed the phonon dispersion calculations for all considered structures. No imaginary phonon frequency was found in the whole Brillouin zone for I-TaB₃, II-TaB₃ and *Amm2*-TaB₄, as shown in Fig. 2, indicating that they are all dynamically stable. Besides, the *Amm2*-TaB₄ is dynamically stable from 0 GPa to their synthetic pressures, which means that they are quenchable to the ambient condition.

3.2 Structure features

Optimized equilibrium lattice parameters, cell volume V of I-TaB₃, II-TaB₃ and *Amm2*-TaB₄ are summarized in Table 1. The crystal structures of I-TaB₃, II-TaB₃ and *Amm2*-TaB₄ are shown in Fig. 3. The monoclinic I-TaB₃ and II-TaB₃ structures both contains four f.u. in a unit cell with lattice parameters of $a = 3.266$ Å, $b = 3.051$ Å, $c = 11.361$ Å, $\beta = 127.947^\circ$ and $a = 3.026$ Å, $b = 5.203$ Å, $c = 9.002$ Å, $\beta = 113.813^\circ$, respectively.

Table 1. Optimized equilibrium lattice parameters (Å and °), cell volume V (Å³), Pressure P (GPa), bulk modulus B (GPa), shear modulus G (GPa), Young's modulus Y (GPa), Poisson's ratio ν , B/G ratio, and hardness (GPa).

Str.	P	a	b	c	β	V	B	G	Y	ν	B/G	H_v
I-TaB ₃	0	3.266	3.051	11.361	127.947	35.99	287	162	408	0.26	1.77	17.02
II-TaB ₃	20	3.026	5.203	9.002	113.813	32.42	299	192	475	0.23	1.56	22.83
TaB ₄	0	9.961	5.285	3.111		40.95	295	219	526	0.20	1.35	30.02

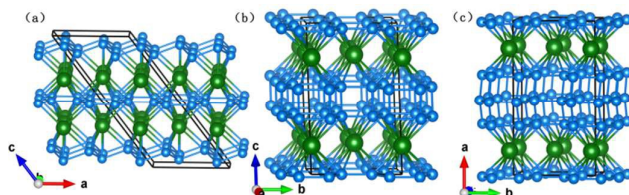


Fig. 3 Crystal structures for (a) I-TaB₃, where the Ta atom occupies the 4i (0.2495, 0.0, 0.6875) and B atoms occupy the 4i (0.6663, 0.0, 0.4996), 4i (0.1508, 0.0, 0.8662) and 4i (0.0827, 0.5, 0.9397) positions, (b) II-TaB₃, where the Ta atom occupies the 4i (0.2380, 0.0, 0.1977), and B atoms occupy the 8j (0.9928, 0.8287, 0.60) and 4g (0.5, 0.1663, 0.0) and (c) *Amm2*-TaB₄, where the Ta atom occupies the 4c (0.8321, 0.0, 0.5282) and B atoms occupy the 8f (0.6596, 0.8294, 0.0401), 4e (0.5, 0.8327, 0.7568) and 4d (0.0, 0.6664, 0.5280). The large green spheres represent Ta atoms and the small blue spheres represent B atoms.

In the I-TaB₃ structure, two puckered hexagonal boron layers extend in one zig-zag crystal plane (Fig. 3a), and Ta atoms are hosted at the channels between two B layers. For high-pressure phase II-TaB₃, it can be described as the alternating a planar graphene-like B layers to *P6/mmm*-TaB₂, and each metal Ta is located in the center of the hexagonal column formed by twelve boron atoms (Fig. 3b). Tantalum tetraboride *Amm2*-TaB₄ contains four f.u. in a unit cell with lattice parameters of $a = 9.961$ Å, $b = 5.285$ Å, $c = 3.111$ Å. Similar to II-TaB₃, *Amm2*-TaB₄ can be viewed to insert two planar hexagonal boron layers in the *P6/mmm*-TaB₂. The *Amm2*-TaB₄ phase has an intriguing B-Ta-B sandwich-like structure constructed with parallel hexagonal graphene-like B layers connected by sp^2 hybridization B-B bonds and Ta layers, forming fundamental TaB₁₂ hexagonal column, as shown in Fig. 3(c).

3.3 Mechanical properties and hardness

In order to further confirm the structural stability of I-TaB₃, II-TaB₃ and *Amm2*-TaB₄, we studied its mechanical stabilities. We calculated the elastic constants using the strain-stress method. All the elastic constants C_{ij} of the considered structures are listed in Table 2. It can be seen that the elastic constants of our predicted two monoclinic phases and an orthorhombic phase satisfy the Born-Huang elastic stability criteria,⁴⁰ and thus these three structures can be mechanically stable. The bulk modulus (B), shear modulus (G), Young's modulus (E), and Poisson's ratio (ν) also be calculated by the known elastic constants as summarized in the Table 1. I-TaB₃ and *Amm2*-TaB₄ have high bulk modulus of 287 GPa and 295 GPa at ambient pressure, which can indicate their strong ability to resist volume deformation. One material with high shear modulus can resist shape change at a constant volume, which can result in high hardness.⁴¹ The *Amm2*-TaB₄ possesses the larger shear modulus of 219 GPa, so its simulated Vickers hardness value (30.02 GPa) is higher than I-TaB₃ at ambient pressure. In addition to the bulk and shear modulus, Poisson's ratio (ν) is an important parameter to indicate the degree of directionality of covalent bonding. The Poisson's ratio (ν) shows the degree of the covalent bonding in directionality. If a material is covalently bound, the ν value is 0.1. For metallic materials, the ν value is 0.33.⁴² Hardness of material is directly affected by the directionality of covalent bonding. From Table 1, we can see that the ν values of considered structures are between 0.20 and 0.26, indicating that these binary borides have both covalent bonding and metallic bonding in structures. The smaller the Poisson's ratio is, the higher the degree of covalent bonding is, and the higher hardness of the material should have. *Amm2*-TaB₄ at ambient condition has the smallest Poisson's ratio (0.20), its hardness is higher than that of I-TaB₃ and II-TaB₃.

Table 2. Calculated elastic constants (GPa) of I-TaB₃, II-TaB₃ and *Amm2*-TaB₄.

Str.	P	C_{11}	C_{22}	C_{33}	C_{44}	C_{55}	C_{66}	C_{12}	C_{13}	C_{23}	C_{15}	C_{25}	C_{35}	C_{46}
I-TaB ₃	0	563	558	716	84	112	211	110	138	137	-6	3	58	-24
II-TaB ₃	20	643	580	464	179	185	229	103	195	209	-5	43	15	-8
<i>Amm2</i> -TaB ₄	0	546	615	642	230	201	211	168	165	91				

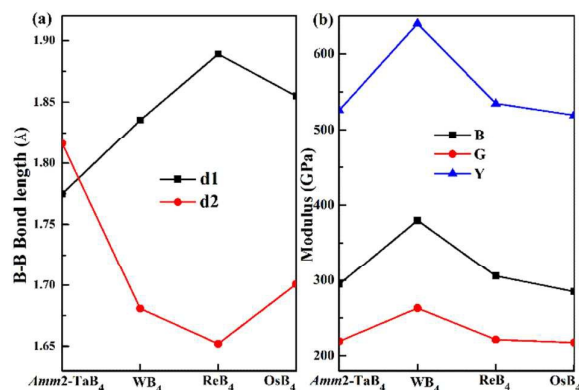


Fig. 4 (a) B-B bond lengths (b) bulk modulus (B), Shear modulus (G), Young's modulus (Y) in TMB_4 . TM represents Ta, W, Re, and Os.

Besides, the stiffness of materials can also be measured by Young's modulus except the bulk modulus, shear modulus and Poisson's ratio. If a kind of material has the larger Young's modulus, it's more difficult for it to be deformed.⁴³ From Table 1, by using Chen's model, the calculated hardness values I-TaB₃ and *Am2*-TaB₄ are of 17.02 and 30.02 GPa, respectively, which are two potential candidates to be ultra-incompressible and hard materials. Besides, High-pressure *Am2*-TaB₄ can be quenched to ambient pressure, so high-pressure can be an effective route to discover other material with excellent mechanical properties.

In order to understand the mechanism of high hardness, the lengths of two kinds of B-B bonds (d1, d2) of *Am2*-TaB₄ are calculated in comparison with other neighboring 5d TMB₄ (TM = W,⁴⁴ Re,⁴⁵ Os⁴⁶). As shown in Fig. S2, d1 represents the average B-B bond length in graphene-like B layers or puckered six-membered-ring boron layers. For OsB₄, d1 represents the average B-B bond length of boron chains paralleling to *b* direction. The d2 represents the average B-B bond length between two B layers or two B chains. Two B-B bond lengths (d1 and d2), bulk modulus (B), Shear modulus (G), and Young's modulus (Y) for TMB₄ (TM = Ta, W, Re, and Os) are shown in Fig. 4. The largest d2 of *Am2*-TaB₄ indicates that the interaction between two layers (graphene-like B layers or puckered six-membered-ring boron layers) in *Am2*-TaB₄ is much weaker than that of other TMB₄. However, the shortest d1 value indicates that *Am2*-TaB₄ has the strongest covalent boron-boron bonds in the graphene-like B layers among the TMB₄ (TM = Ta, W, Re, and Os). The average effect of d1 and d2 make the *Am2*-TaB₄ have the similar B , G , and Y values to ReB₄, and OsB₄. The B-B covalent bonds in graphene-like layers mainly make *Am2*-TaB₄ have high hardness.

3.4 Electronic Structure

In order to understand the origin of physical properties of materials, it is important to know the electronic structure of material. So we calculated the total and partial density of states (PDOS) as shown in the Fig. 5. It is found that all considered structures are metallic material because of the finite DOS at the Fermi level (E_F). From the PDOS of them, the tantalum 5d states and boron 2p states contribute to the most part of DOS, and the boron 2s states are mainly situated at the bottom of the valence bands. From the PDOS of them, it also can be found that the orbits of Ta-5d and B-2p profiles are very similar, re-

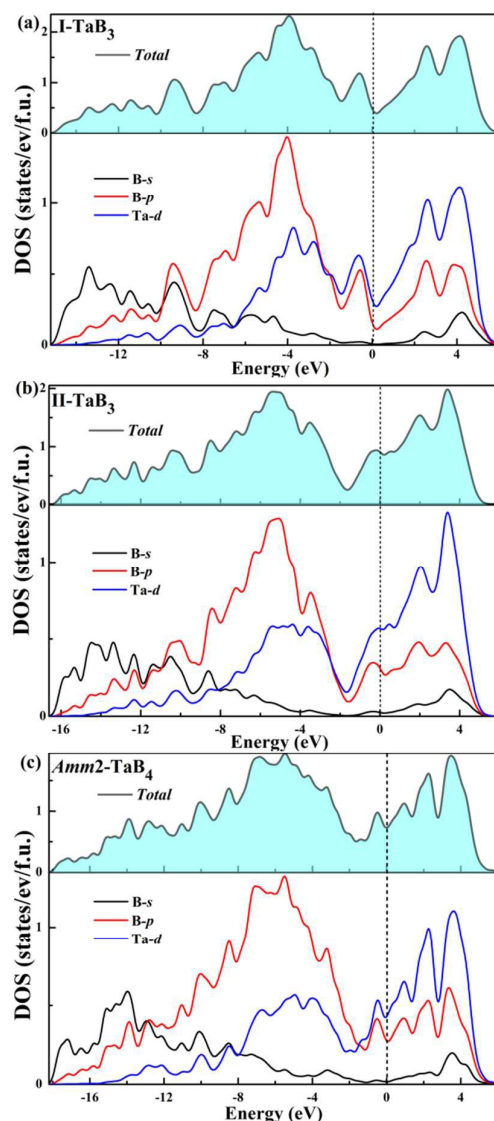


Fig. 5 Calculated total (TDOS) and partial density of states (PDOS) of (a) I-TaB₃, (b) II-TaB₃ and (c) *Am2*-TaB₄.

flecting the orbital hybridization between Ta and B atoms. The hybridization between Ta-*d* and B-*p* electrons is very important for the incompressibility and high hardness. The typical feature of *C2/m*-TaB₃ and *Am2*-TaB₄ is that there is a pseudo-gap at the Fermi level, which is termed as the borderline between the bonding and anti-bonding states⁴⁷ and is helpful for stabilizing the Ta-B structures.

For *Am2*-TaB₄, we have made a clear comparison with a 3d boride (*Am2*-VB₄)⁴⁸ and a 4d boride (*P6₃/mmc*-RuB₄)⁴⁹ for the part of electronic properties and chemical bonding. As shown in Fig. S3, three transition metal borides have electronic hybridizations between B-*p* and TM-*d* orbitals (TM = V, Ru, and Ta). The hybridization of *Am2*-TaB₄ is very important for the structural stability and incompressibility, which is similar to other 3d or 4d borides.

3.5 Chemical Bonding

In order to understand the bonding character of these compounds in detail, we calculated the electronic localization function (ELF)⁴⁵ to study the bonding feature of *C2/m*-TaB₃ and *Amm2*-TaB₄, shown in Fig. 6. Using the ELF calculation, we can get the bonding type of materials such as metallic,

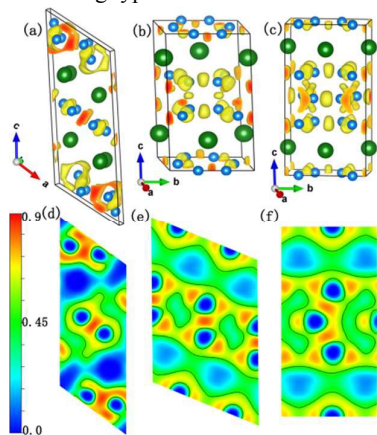


Fig. 6 Contours of ELF = 0.75 of I-TaB₃(a), II-TaB₃(b) and *Amm2*-TaB₄(c) and (010) plane of I-TaB₃(d), II-TaB₃(e) and *Amm2*-TaB₄(f).

covalent or ionic bonding. The ELF is a contour plot which is composed of different contours values in range of 0 and 1, $elf = 1$ suggests the perfect electron-localization, $elf = 0.5$ suggests electron-gas-like pair probability and $elf = 0$ suggests complete non-electron-localization. We plot the contours of the ELF = 0.75 and (010) plane for I-TaB₃, II-TaB₃ and *Amm2*-VB₃ (Fig. 6), respectively. High electron localization can be seen in the region between B atoms, indicating strong covalent B-B bonding. Meanwhile, ELF is negligible at the Ta sites, whereas ELF between Ta and B atoms attains local maximum values very close to the B sites, indicating partially covalent and ionic interactions between Ta and B atoms. Above discussion, II-TaB₃ and *Amm2*-TaB₄ have the similar structural features. Then we can see that ELF between six-membered ring layers of *Amm2*-TaB₄ is stronger than II-TaB₃, by comparing Fig. 6(b) and 6(c).

To gain a further insight into the B-B bonding mechanism of *Amm2*-TaB₄, electronic localization function (ELF) comparing with *P6₃/mmc*-RuB₄ was calculated, as shown in Fig. S4. There is strong electron localization between the B–B atoms, reflecting the strong covalent bonding. For *Amm2*-TaB₄, ELF in A, B, C layers shows higher values than the others, contributing to greater C_{22} (615 GPa) and C_{33} (642 GPa) than C_{11} (546 GPa). Although, the C_{33} (833 GPa) of *P6₃/mmc*-RuB₄⁴⁹ is larger, the values of B (295 GPa) and G (219 GPa) of *Amm2*-TaB₄ are larger than that of *P6₃/mmc*-RuB₄⁴⁹ (B 281 GPa, G 175 GPa) (Table. S1). It indicates that total B–B interaction in the graphene-like layers in *Amm2*-TaB₄ is stronger than total puckered B–B bond of *P6₃/mmc*-RuB₄. So, for *Amm2*-TaB₄, strong B-B covalent bonds in graphene-like B layers and between layers make it have outstanding mechanical properties.

4 Conclusions

In conclusion, structure searches based on first-principles calculations discover three stable structures: one ground-state monoclinic TaB₃, a high-pressure monoclinic TaB₃ and an orthorhombic *Amm2*-TaB₄. These three boron-rich tantalum borides are dynamically and elastically stable. The observations of structural and elastic characteristic for *Amm2*-TaB₄ show that it has superior mechanical properties. The estimated Vickers hardness values are 30.2 GPa for *Amm2*-TaB₄ at ambient pressure. This suggests that *Amm2*-TaB₄ is potentially low compressible and hard materials. Analysis of electronic structure and chemical bonding indicate that the strong covalent and directional B-B bonds in graphene-like B layers and between layers of *Amm2*-TaB₄ have significant effect on its stability and great mechanical properties. We update the phase diagram of Ta-B system and we hope that our present theoretical investigation may provide a further experimental realization of boron-rich transition metal borides.

Acknowledgments

This work was supported by the National Basic Research Program of China (No. 2011CB808200), National Natural Science Foundation of China (Nos. 51572108, 11404134, 51032001, 11204100, 11574109), Program for Changjiang Scholars and Innovative Research Team in University (No. IRT1132), National Found for Fostering Talents of basic Science (No. J1103202), and China Postdoctoral Science Foundation (2014M561279). Part of calculations were performed in the High Performance Computing Center (HPCC) of Jilin University.

References

- 1 E. Gregoryanz, C. Somayazulu, M. Badro, J. Fiquet, G. Mao, H.-k. Mao and R. J. Hemley, *Nat. Mater.*, 2004, **3**, 294–297.
- 2 J. C. Crowhurst, A. F. Goncharov, B. Sadigh, C. L. Evans, P. G. Morrall, J. L. Ferreira and A. J. Nelson, *Science*, 2006, **311**, 1275–1278.
- 3 A. F. Young, C. Sanloup, E. Gregoryanz, S. Scandolo, R. Hemley and H.-k. Mao, *Phys. Rev. Lett.*, 2006, **96**, 155501.
- 4 H. Gou, N. Dubrovinskaia, E. Bykova, A. A. Tsirlin, D. Kasinathan, W. Schnelle, A. Richter, M. Merlini, M. Hanfland, A. M. Abakumov, D. Batuk, G. Tendeloo, Y. Van Nakajima, A. N. Kolmogorov and L. Dubrovinsky, *Phys. Rev. Lett.*, 2013, **111**, 157002.
- 5 H.-Y. Chung, M. B. Weinberger, J. B. Levine, A. Kavner, J.-M. Yang, S. H. Tolbert and R. B. Kaner, *Science*, 2007, **316**, 436–439.
- 6 R. W. Cumberland, M. B. Weinberger, J. J. Gilman, S. M. Clark, S. H. Tolbert and R. B. Kaner, *J. Am. Chem. Soc.*, 2005, **127**, 7264–7265.
- 7 R. Mohammadi, M. Xie, A. T. Lech, C. L. Turner, A. Kavner, S. H. Tolbert and R. B. Kaner, *J. Am. Chem. Soc.*, 2012, **134**, 20660–20668.
- 8 H. Niu, J. Wang, X. Q. Chen, D. Li, Y. Li, P. Lazar, R. Podloucky and A. N. Kolmogorov, *Phys. Rev. B: Condens. Matter Mater. Phys.*, 2012, **85**, 144116.
- 9 P. F. McMillan, *Nat. Mater.*, 2002, **1**, 19–25.
- 10 X. Zhang, J. Qin, X. Sun, Y. Xue, M. Ma and R. Liu, *Phys. Chem. Chem. Phys.*, 2013, **15**, 20894–20899.
- 11 Y. Pan, W. T. Zheng, W. M. Guan, K. H. Zhang and X. F. Fan, *J. Solid*

- State Chem.*, 2013, **207**, 29-34.
- 12 A. N. Kolmogorov, S. Shah, E. R. Margine, A. F. Bialon, T. Hammerschmidt and R. Drautz, *Phys. Rev. Lett.*, 2010, **105**, 217003.
- 13 R. Kiessling, *Acta Chem. Scand.*, 1949 **3**, 603-615.
- 14 A. G. Van Der Geest and A. N. Kolmogorov, *Calphad*, 2014, **46**, 184-204.
- 15 X. Zhang, G. E. Hilmas and W. G. Fahrenholtz, *Mater. Lett.*, 2008, **62**, 4251-4253.
- 16 J. D. Zhang, X. L. Cheng and D. H. Li, *Comp. Mater. Sci.*, 2010, **50**, 474-478.
- 17 C. L. Yeh and H. J. Wang, *Ceram. Int.*, 2011, **37**, 1569-1573.
- 18 T. Yao, Y. Wang, H. Li, J. Lian, J. Zhang and H. Gou, *Comp. Mater. Sci.*, 2012, **65**, 302-308.
- 19 R. Heid, B. Renker, H. Schober, P. Adelman, D. Ernst and K. P. Bohnen, *Phys. Rev. B*, 2003, **67**, 180510.
- 20 W. J. Zhao and Y. X. Wang, *J. Solid State Chem.*, 2009, **182**, 2880-2886.
- 21 B. Chu, D. Li, K. Bao, F. Tian, D. Duan, X. Sha, P. Hou, Y. Liu, H. Zhang, B. Liu and T. Cui, *J. Alloys Comp.*, 2014, **617**, 660-664.
- 22 X. Zhang, E. Zhao and Z. Wu, *J. Alloys Comp.*, 2015, **632**, 37-43.
- 23 A. R. Oganov, Y. M. Ma, A. O. Lyakhov, M. Valle and C. Gatti, *Rev. Mineral. Geochem.*, 2010, **71**, 271-298.
- 24 A. R. Oganov and C. W. Glass, *J. Chem. Phys.*, 2006, **124**, 244704.
- 25 A. R. Oganov, A. O. Lyakhov and M. Valle, *Acc. Chem. Res.*, 2011, **44**, 227-237.
- 26 A. O. Lyakhov, A. R. Oganov, H. T. Stokes and Q. Zhu, *Comput. Phys. Commun.*, 2013, **184**, 1172-1182.
- 27 G. Kresse and J. Furthmüller, *Phys. Rev. B*, 1996, **54**, 11169-11186.
- 28 J. P. Perdew, K. Burke and M. Ernzerhof, *Phys. Rev. Lett.*, 1996, **77**, 3865-3868.
- 29 D. Li, F. Tian, D. Duan, K. Bao, B. Chu, X. Sha, B. Liu and T. Cui, *RSC Adv.*, 2014, **4**, 10133-10139.
- 30 D. Li, Bao, K; F. Tian, B. Chu, D. Duan, X. Sha, Y. Lv, H. Zhang, N. Lu, B. Liu and T. Cui, *Scientific Reports*, 2015, **5**, 13447.
- 31 D. Li, K. Bao, F. Tian, Z. Zeng, Z. He, B. Liu and T. Cui, *PCCP*, 2012, **14**, 4347-4350.
- 32 R. Hill, *Proc. Phys. Soc. London, Sect.*, 1952, **65**, 349-354.
- 33 K. Parlinski, Z. Q. Li and Y. Kawazoe, *Phys. Rev. Lett.*, 1997, **78**, 4063-4066.
- 34 A. Togo, F. Oba and I. Tanaka, *Phys. Rev. B: Condens. Matter Mater. Phys.*, 2008, **78**, 134106.
- 35 X. Q. Chen, H. Niu, D. Li and Y. Li, *Intermetallics*, 2011, **19**, 1275-1281.
- 36 A. R. Oganov, J. H. Chen, C. Gatti, Y. Z. Ma, Y. M. Ma, C. W. Glass, Z. X. Liu, T. Yu, O. O. Kurakevych and V. L. Solozhenko, *Nature*, 2009, **457**, 863-867.
- 37 M. G. Zhang, H. Wang, H. Wang, T. Cui and Y. Ma, *J. Phys. Chem. C*, 2010, **114**, 6722-6725.
- 38 G. Ghosh, A. van de Walle and M. Asta, *Acta Mater.*, 2008, **56**, 3202-3221.
- 39 X. W. Zhang, G. Trimarchi and Zunger, *Phys. Rev. B*, 2009, **79**, 092102.
- 40 Z. J. Wu, E. J. Zhao, H. P. Xiang, X. F. Hao, X. J. Liu and J. Meng, *Phys. Rev. B*, 2007, **76**, 054115.
- 41 J. S. Tse, *J. Superhard Mater.*, 2010, **32**, 177-191.
- 42 S. F. Pugh, *Philos. Mag.*, 1954, **45**, 823-843.
- 43 M. Born, *Mathematical Proceedings of the Cambridge Philosophical Society*, 2008, **36**, 160.
- 44 Q. Li, D. Zhou, W. T. Zheng, Y. M. Ma, C. F. Chen, *Phys. Rev. Lett.* 2013, **110**, 136403.
- 45 B. Wang, D.Y. Wang, Y.X. Wang, *J. Alloys Compd.*, 2013, **573**, 20-26.
- 46 M. Zhang, H. Yan, G. Zhang, H.J. Wang, *J. Phys. Chem. C*, 2012, **116**, 4293-4297.
- 47 P. Vajeeston, P. Ravindran, C. Ravi and R. Asokamani, *Phys. Rev. B: Condens. Matter Mater.*, 2001, **63**, 045115.
- 48 L. Wu, B. Wan, Y. Zhao, Y. Zhang, H. Liu, Y. Wang, J. Zhang, H. Gou, *J. Phys. Chem. C* 2015, **119**, 21649-21657.
- 49 Y. Wang, T. Yao, L.-M. Wang, J. Yao, H. Li, J. Zhang, H. Gou, *Dalton Trans.* 2013, **42**, 7041-7050.
- 50 A. Savin, J. Flad, H. Preuss and H. G. von Schnering, *Angew. Chem. Int. Ed. Engl.*, 1992, **31**, 185-187.